HHS Public Access

Author manuscript

Nature. Author manuscript; available in PMC 2010 November 01.

Published in final edited form as:

Nature. 2010 May 13; 465(7295): 188–193. doi:10.1038/nature09057.

Single-molecule dynamics of gating in a neurotransmitter transporter homolog

Yongfang Zhao[1,2,4,7], **Daniel Terry**[5,7], **Lei Shi**[5,6], **Harel Weinstein**[5,6], **Scott C. Blanchard**[5,☎], and **Jonathan A. Javitch**[1,2,3,4,☎]

[1]Center for Molecular Recognition, Columbia University College of Physicians and Surgeons, 630 W. 168th, New York, New York 10032, USA.

[2]Department of Psychiatry, Columbia University College of Physicians and Surgeons, 630 W. 168th, New York, New York 10032, USA.

[3]Department of Pharmacology, Columbia University College of Physicians and Surgeons, 630 W. 168th, New York, New York 10032, USA.

[4]Division of Molecular Therapeutics, New York State Psychiatric Institute, New York, NY 10032, USA.

[5]Department of Physiology and Biophysics, Weill Cornell Medical College, 1300 York Avenue, New York, NY 10021, USA.

[6]HRH Prince Alwaleed Bin Talal Bin Abdulaziz Alsaud Institute for Computational Biomedicine, Weill Cornell Medical College, 1300 York Avenue, New York, NY 10021, USA.

Summary

Neurotransmitter:Na^+ symporters (NSS) remove neurotransmitters from the synapse in a reuptake process driven by the Na^+ gradient. Drugs that interfere with this reuptake mechanism, such as cocaine and antidepressants, profoundly influence behavior and mood. In order to probe the nature of conformational changes associated with substrate binding and transport, we have developed a single-molecule fluorescence imaging assay, in combination with functional and computational studies, using the prokaryotic NSS homolog LeuT. Here we show molecular details of the modulation of intracellular gating of LeuT by substrates and inhibitors, as well as by mutations that alter binding and/or transport. Our direct observations of single-molecule transitions, reflecting structural dynamics of the intracellular region of the transporter that may be masked by

☎Jonathan A. Javitch, M.D., Ph.D., Columbia University College of Physicians and Surgeons, Center for Molecular Recognition, 630 West 168th Street, P&S 11-401, New York, NY 10032, USA; Phone: 212-305-3974; Facsimile: 212-305-5594; jaj2@columbia.edu.
☎Scott C. Blanchard, Ph.D. Department of Physiology and Biophysics, Weill Cornell Medical College, 1300 York Avenue, New York, NY 10021, USA. Phone: 212-746-6163; Facsimile: 212-746-4843; scb2005@med.cornell.edu.
[7]These authors contributed equally.

Author Contributions: YZ expressed, purified, labeled, and functionally characterized the LeuT mutants. YZ and DT designed, carried out, and analyzed the single-molecule experiments. LS and HW designed and analyzed the computational studies, which were carried out by LS. SCB and JAJ helped to design the biochemical and single-molecule experiments and with LS and HW helped interpret the data. All the authors contributed to writing and editing the manuscript.

Supplementary Information is linked to the online version of the paper at www.nature.com/nature.

ensemble averaging or suppressed under crystallographic conditions, are interpreted in the context of an allosteric mechanism coupling ion and substrate binding to transport.

The neurotransmitter:Na^+ symporter (NSS) family terminates cellular signaling by recapturing released neurotransmitter1–3. These secondary active transporters enable the thermodynamically uphill transport of their respective substrates across the plasma membrane of the presynaptic neuron in a co-transport (symport) mechanism driven by the Na^+ electrochemical gradient4–6. The transporters for the biogenic amines, dopamine, norepinephrine, and serotonin, are of particular interest because they are targeted by numerous drugs, including the widely abused psychostimulants cocaine and amphetamine1, as well as antidepressants7. Genes encoding more than 200 putative NSS homologs have been identified in prokaryotic genomes8. The crystal structure of LeuT9, a prokaryotic NSS homolog from the thermophile *Aquifex aeolicus* comprised of 12 transmembrane helices, revealed an occluded state in which one leucine (Leu) and two Na^+ ions are bound deep within the protein (Fig. 1). When reconstituted into proteoliposomes, LeuT mediates Na^+-dependent transport of Leu and Ala at rates of ~0.1–0.4/min10. Computational and experimental studies identified a key mechanistic role for a second substrate binding site in the extracellular vestibule, comprised of many of the same residues shown to interact with antidepressants11–13. The two binding sites can be occupied simultaneously, and substrate in the second site (S2) allosterically triggers intracellular release of Na^+ and substrate from the primary site (S1)10. In contrast, tricyclic antidepressants (TCAs), which also bind in the S2 site (Fig. 1), do not promote substrate release from the S1 site. Instead, TCAs competitively block substrate binding to the S2 site and inhibit transport. Thus, the allosteric changes in LeuT induced by substrate binding to the S2 site must differ from those, if any, produced by TCAs.

Notably, the crystal structures of LeuT with and without TCA bound are almost identical. Moreover, all LeuT structures to date have been solved in the detergent n-octyl-β-D-glucopyranoside (OG)9,11,12,14, whereas functional studies of LeuT have been carried out with protein purified in the detergent n-dodecyl-β-D-maltopyranoside (DDM)9–12,14. Like TCAs, OG competes with substrate binding to the S2 site and disrupts the Na^+-coupled symport mechanism15. Thus, all available LeuT structures are likely to represent functionally blocked states in which allosteric changes related to function may be difficult or impossible to discern.

To probe the nature of the conformational changes associated with substrate binding and transport, we have undertaken an integrated approach including functional, computational and single-molecule fluorescence imaging assays. Time-dependent changes in LeuT structure, potentially masked by ensemble averaging in bulk measurements or suppressed through crystallographic conditions, were observed experimentally and quantified16 using single-molecule fluorescence resonance energy transfer (smFRET) methods17–28. The mechanistic context of the observed conformational changes in LeuT was assessed computationally using molecular dynamics simulations related to the functional assays10,15,29–33. Here, we focused on understanding conformational events on the

intracellular side of LeuT, as major conformational changes in this region have not been revealed through crystallographic means but are required for inward substrate release.

Single-molecule experiments were performed on single and double cysteine (Cys) LeuT mutants, linked to fluorophores through maleimide chemistry. Cys residues were introduced into LeuT, which lacks native Cys, at non-conserved positions that were shown to be distal to the established ligand binding sites and solvent accessible based on crystal structures and MD simulations. LeuT mutants chosen for investigation were also selected based on efficient fluorophore coupling (>80–90%) and low nonspecific labeling (< 4%) (Supplementary Fig. 1), low anisotropy parameters (Supplementary Table 1) and wild-type-like proteoliposome-reconstituted transport activity (Supplementary Table 2). Six Cys pairs on the intracellular side of the transporter were shown to be suitable for imaging experiments based on these criteria. These included combinations of Cys substitutions for His7 in the N-terminus, Arg86 in IL1, Arg185 in IL2, Lys271 in IL3, and Thr515 at the cytoplasmic end of TM12. To obtain comparative measures of motion, one Cys pair (positions Lys239 in EL3 and His480 in EL6) was also selected on the extracellular surface of LeuT (Fig. 1).

smFRET experiments were initially performed on N-terminally His-tagged, Cy3/Cy5-labeled LeuT in 0.03% DDM, surface immobilized through a biotin-NTA interaction within passivated, streptavidin-coated microfluidic chambers34,35 (Fig. 2, Supplementary Fig. 2). By controlling the density of surface immobilization through dilution and using a prism-based, wide-field configuration, low-density arrays of specifically-tethered, individual LeuT molecules could be imaged simultaneously. As described elsewhere36, oxygen scavenging and triplet state quenching conditions for optimal fluorophore performance (low photophysical noise and reduced photobleaching) were achieved through screening (Supplemental Methods). Initial measurements of H7C/R86C- and H7C/T515C-labeled LeuT molecules, performed at 40 ms time resolution and high signal-to-noise ratio (~18:1 on average), showed that both systems, in the presence of 200 mM K^+ and the nominal absence of Na^+, displayed two readily distinguished FRET states (~0.51 and ~0.75; ~0.43 and ~0.73, respectively) (Fig. 2b, c, d, Supplementary Fig.3). Such observations suggested the existence of two distinct LeuT conformations in the population differing by ~13 Å in the distance between each fluorophore pair (Supplemental Table 3). (Note that the short-lived, zero-FRET state sampling events correspond to transient excursions of the Cy5 fluorophore to non-fluorescent dark states.)

Consistent with the EC_{50} of Na^+ for stimulating binding and transport (~10 mM)10, and a ligand-dependent transition between these states, the relative populations of low- and high-FRET LeuT conformations were dependent on Na^+ concentration. Addition of saturating Na^+ concentrations (200 mM) stabilized higher-FRET states in both systems (~0.77 and ~0.73, for H7C/R86C and H7C/T515C, respectively) (Fig. 2, Supplementary Table 3, Supplementary Fig. 3), consistent with substrate-bound LeuT crystal structures, where the intracellular end of the transporter is observed to be compact9,14. High-FRET state occupancy was saturated at 200 mM Na^+. Under such conditions, further changes in FRET were not observed upon addition of 20 μM Leu (Fig. 2, Supplementary Table 3). However, at 5 mM Na^+, where both low- and high-FRET states remain populated, Leu binding

redistributed the two populations in a concentration-dependent fashion in favor of higher-FRET configurations (Fig. 2e, f). The same results were obtained whether LeuT molecules were immobilized via the N- or the C-terminus.

These findings are consistent with spontaneous, ligand-modulated rearrangements in specific elements of LeuT near the intracellular gating region. In the absence of ligands a low-FRET state would be achieved by either an outward and/or downward movement of position 7 (at the N-terminus of TM1) with respect to positions 86 (IL1) and 515 (cytoplasmic end of TM12). Correspondingly, a high-FRET state may be achieved spontaneously or upon ligand binding by a reciprocal motion of TM1 with respect to IL1/TM12, leading to an inward-closed LeuT conformation. In contrast, substrate-dependent changes were not observed for any of the other constructs labeled on the intracellular face of the protein (Supplementary Fig. 4), suggesting that these positions do not move substantially during intracellular gating.

The site of labeling at position 7 is adjacent to the highly conserved Trp8 residue, which is involved in a conserved interaction network among a residue triad including Ile187 (IL2) and Tyr268 (IL3) at the intracellular face (Supplementary Fig. 5)32. Tyr268 also forms cation-π and ionic interactions with residues Arg5 (NT) and Asp369 (TM8), thus serving to bring together NT, IL2, and IL3 and closing the transport pathway at the intracellular surface of LeuT (Fig. 1). Mutation of the homologous interaction network in the structurally-related dopamine transporter and GABA transporter has been inferred to promote inward-open conformations32,37.

To interpret the distance changes identified with smFRET with respect to changes occurring in the intracellular interaction network during the transition from an outward-open to an inward-open conformation, and to investigate how they may pertain to the transport mechanism, molecular dynamics (MD) simulations were performed. Inward-open conformations of LeuT previously generated by computationally “pulling” the S1 site-bound substrate intracellularly in the presence of S2 and absence of Na210, were subjected to prolonged MD simulations (two parallel runs of 150 ns each), designed to examine the structural equilibration of LeuT following the simulated substrate transport event. During the extended equilibration period, we observed dissociation of the Trp8-Ile187-Tyr268 interaction network. This resulted in a relative downward and outward movement of TM1 and the region containing the residue at position 7, and a corresponding increase in the distance between positions 7 and 86 (Fig. 3, Supplementary Movie I, II) and position 7 and the intracellular end of TM12 (Supplementary Fig. 6). This rearrangement was associated with significant conformational changes in the IL2-TM5 region (including Ile187), facilitated by changes in bend angle of the highly-conserved proline-kink in TM5. In contrast, the distance between residues 86 and 185 was largely unchanged throughout the simulation (Fig. 3) as the bottom of TM4 maintained a relatively stable position.

Thus, the conformational rearrangements in LeuT observed during the simulated transport event leading to the inward-open conformation were found to be in good agreement with the estimated changes in distance deduced from the smFRET data. A recent analysis of crystal structures sharing a LeuT-like fold prompted Gouaux and colleagues to propose that

coordinated rearrangements of TM1a and TM1b are associated with conformational transitions in the protein38. Both our simulation and smFRET data are in line with a movement of TM1a as shown in Fig. 3 (see also Supplementary Movie I, II) and illuminate the function-related dynamic elements in these putative rearrangements. Importantly, as can be seen in Fig. 3 and Supplemental Movie 1, an outward movement of TM1a is essential to create space for Leu to be released to the cytoplasm.

To examine further how the interaction network at the intracellular end of LeuT contributes to the inward-open conformation, smFRET experiments were performed on H7C/R86C-labeled LeuT constructs in the background of the disruptive mutations, R5A or Y268A32. As anticipated, lower-FRET states were observed for both mutant constructs in the absence of Na^+ (Fig. 4). In both cases, the absolute values of the low-FRET states (~0.43 and ~0.44, respectively) were significantly lower than observed for the wild-type background (~0.51) (Supplementary Table 3). These observations suggest that the low-FRET state visited in the wild-type background in the absence of Na^+ may represent a time-averaged population of low-FRET configurations that change in the context of the R5A and Y268A mutations.

Both mutations also affected the FRET distributions observed for extracellularly-labeled LeuT (K239C/H480C), suggesting that the “inward opening” effects of these mutations are coordinated with “outside closing.” Allosteric effects were also observed in response to the mutation of Arg30, which lines the S2 site10 and participates in the formation of cation-π interactions within a proposed extracellular “gating region”9. In the R30A mutant, H7C/R86C-labeled LeuT was observed to adopt a high-FRET configuration in the absence of Na^+ (~0.70), whereas the distance between extracellular pairs (K239C/H480C) was unchanged (Fig. 4, Supplementary Table 3). These data, corroborated by evidence from the H7C/T515C construct (Supplementary Fig. 3), show that mutations in putative intracellular and extracellular gate regions lead to long-range effects on the conformation of LeuT. However, that the R30A mutation affected the conformation of the intracellular network, while leaving the extracellular probes largely unchanged, suggests that the transmission of signal throughout the molecule involves a cascade of flexible interactions and local conformations rather than a single rigid body rearrangement10,32,39.

Also consistent with an allosterically-mediated modulation of the interaction network in the intracellular side, the TCA inhibitor, clomipramine (CMI), was observed to stabilize a high-FRET state (~0.69) in wild-type H7C/R86C-labeled LeuT (Fig. 4). This FRET value, distinct from that observed in the absence of CMI (~0.75), was unchanged in the presence of Na^+ (Supplementary Table 3), a result that agrees with the MD simulations of LeuT (>100 ns trajectory) performed with either CMI or OG present in the S2 site (and Leu in the S1 site)15. These experiments showed that the intracellular network adopted similar and slightly more open configurations when CMI or OG was present in the S2 site, approximately 30 Å away from residue 7 at the intracellular end of TM1 (Supplementary Fig. 7). On the extracellular side, experiments showed that CMI increased FRET between K239C/H480C-labels (from ~0.49 to ~0.53) (Fig. 4), consistent with a modest compaction of this region of LeuT when inhibitor was bound.

To examine directly whether the conformational changes associated with intracellular gating could be tracked in individual LeuT molecules, smFRET experiments were performed under conditions supporting extended imaging time scales. First, the laser illumination intensity was reduced to minimize the photobleaching that had previously limited the observation window (~3 s). Second, the exposure time was increased 4-fold to 160 ms to maintain signal-to-noise ratios adequate to detect FRET changes at reduced laser intensity. Finally, to eliminate the spontaneous dissociation of LeuT from the image plane that resulted from the relatively low-affinity His-NTA interaction (k_{off} >0.25 min^{-1}), a 15 amino acid, C-terminal biotinylation domain40 was introduced into the LeuT (H7C/R86C) construct to allow immobilization via a biotin-streptavidin linkage much less prone to dissociation (k_{off} < 0.25 h^{-1}) (data not shown).

Given the benefit of an extended observation period, individual LeuT-H7C/R86C molecules could be shown to exhibit multiple transitions between the high- and low-FRET configurations in the absence of Na^+ (Fig. 5a), consistent with the direct detection of isomerization of the intracellular network. With the reduced illumination intensity, the low-FRET state exhibited short-lived photophysical “blinking” events that were likely masked under intense illumination due to rapid, Cy3-mediated photoresurrection36 (see Supplementary Discussion). Taking this into consideration, the average dwell time in high (τ ~18 s) and low (τ ~25 s) FRET states could be estimated, suggesting that a full opening-closing cycle required ~60 s. As anticipated from the results obtained in shorter time scale experiments, the high FRET state was highly stabilized in the presence of high Na^+ concentrations (> 76 sec, limited by photobleaching) (Fig. 5b, c).

The unique behaviors of R5A and Y268A LeuT mutants could also be assessed in greater detail under long time-scale imaging conditions. LeuT-Y268A predominantly exhibited a single, broadened low-FRET state in the absence of Na^+ (Fig. 5e). Transitions to higher-FRET states were very rare, both in the absence and presence of substrates. However, consistent with Na^+ binding and partial/incomplete gate closure, the lower-FRET state value increased in the presence of saturating Na^+ and Leu (Fig. 5f, g). In light of the dramatically impaired transport activity of LeuT-Y268A (Supplementary Fig. 8), these data suggest a potential correlation between the ability to achieve a properly closed intracellular interaction network and the efficiency of transport. They are also in agreement with our previous suggestion that the Y335A dopamine transporter (homologous to LeuT Y268A), has low transport activity because it adopts an inward-open conformation32. Interestingly in this mutant, zinc, which is thought to help the transporter reach an outward-facing conformation, dramatically enhances transport32, presumably by facilitating inward closure.

LeuT-R5A showed transient, Leu-dependent isomerization to high-FRET configurations for the 7/86 pair (~0.77), consistent with an inward closed conformation (compare Fig. 5i, k) and with its much less impaired transport activity compared to Y268A (Supplementary Fig. 8). As for LeuT-Y268A, Na^+ alone served only to shift the low-FRET state value slightly higher. With both substrates present, the lower-FRET state dwell time was similar to that of the wild-type background (τ ~ 28 s), whereas the lifetime of the high-FRET state was substantially reduced compared to the wild-type background (τ ~8 s vs. ~18 s, respectively).

In summary, our MD and smFRET data indicate that a movement of TM1a is associated with intracellular gating in LeuT. This movement is regulated by substrate and inhibitor binding, by mutations of the intracellular network that stabilizes an inward-closed state, and by mutations of the S2 site, reflecting the allosteric nature of the transport mechanism. While FRET-based single-molecule studies using a confocal imaging approach have previously identified distinct conformational states in the H^+-coupled sugar transporter lactose permease41,42, the minutes-long time scale FRET trajectories obtained here, directly revealing relatively slow conformational switching events in LeuT, would be difficult or impossible to observe using other methods. The extension of imaging times beyond the limit of freely-diffusing molecules using the TIR approach, in combination with the surface-immobilization and triplet state quenching strategies employed, provide a powerful new means to explore the structural and kinetic features of Na^+:substrate symport by LeuT. Extension of these single-molecule imaging approaches to other membrane proteins, as well as to LeuT reconstituted into proteoliposomes in which we can control the Na^+ gradient, will provide further mechanistic details on how the energy stored in ion gradients can be used to drive uphill substrate accumulation by secondary active transporters.

Methods Summary

LeuT mutants were expressed in *E. coli*, purified, and labeled on targeted engineered cysteines with Cy3 and Cy5 maleimide. The functional properties of the labeled constructs were determined by measuring Leu binding by scintillation proximity assay, and Ala transport was measured after reconstitution of the protein into proteoliposomes. The fluorescence properties of labeled proteins were studied to establish specific and efficient labeling and to establish that the observed FRET changes likely arise from inter-dye distance rather than photophysical phenomena. Various constructs were created, each with two cysteine residues strategically placed for labeling. Purified, labeled protein was immobilized onto a passivated-glass surface *via* a streptavidin-biotin linkage. Fluorescence data were acquired using a prism-based total internal reflection (TIR) microscope. Fluorescence resonance energy transfer (FRET) efficiency was calculated and analysis of fluorescence and FRET traces was achieved using automated analysis software developed for this application. The single molecule traces were analyzed for LeuT in the presence and absence of the substrates sodium and Leu, upon addition of the transport inhibitors clomipramine and octylglucoside, and in response to mutations of the extracellular vestibule as well as the network of intracellular residues proposed to stabilize the inward closed state. Molecular dynamics simulations of the protein immersed in an explicit membrane, solvated with water molecules, ions and ligands, were carried out and long equilibrations (totaling >500 ns) were run to assess conformational changes.

Methods

Protein expression and purification

Wild-type and mutant LeuT were produced in *E. coli* C41(DE3) harboring pQO18 or pET16b and purified by immobilized metal (Ni^{2+}) affinity chromatography using a Ni^{2+} Sepharose 6 FastFlow column (GE Healthcare). The preparation of membrane vesicles and the subsequent purification of LeuT variants were performed as described43. For Cy3 or

Cy5 labeled protein, after the protein was immobilized on the Ni^{2+} Sepharose 6 FastFlow resin, the resin was washed with 5 column volumes of Buffer A: 50mM Tris/Mes (pH 7.5), 150 mM NaCl, 1mM TCEP, 20% Glycerol, 0.05 % [wt/vol] (1 mM) *n*-dodecyl-β-d-maltopyranoside (DDM), and 50 mM imidazole. The resin was then washed with 5 column volumes of labeling buffer: 50 mM Mes (pH 6.0), 400 mM NaCl, 200 uM lysine, 50 μM TCEP, 1 mM DDM. After resuspending the resin in labeling buffer, 200 μM Cy3 and 200 μM Cy5 maleimide (GE healthcare) were added to the solution and reacted for 1 hour at 4°C while rotating the column. To remove free Cy3 and Cy5, the resin was reloaded into the column and washed with 5 column volume of buffer A. The protein was eluted in Buffer A with 300 mM imidazole and purified with HPLC-mediated size-exclusion chromatography (Shodex Protein-KW803 column) in Buffer B: 50 mM Tris/Mes (pH 7.5), 150 mM NaCl, 1 mM TCEP, 1 mM DDM.

The extent of the labeling was estimated from absorption spectra of labeled protein by measuring peak maxima at 552 nm and 650 nm for Cy3 and Cy5, respectively, using a Hitachi model 24 UV-VIS scanning spectrophotometer (Hitachi, Japan). Protein concentration was determined by the amido black method44. Under the same conditions, control labeling experiments of wild-type LeuT, which is devoid of cysteine, resulted in no significant incorporation of Cy3 or Cy5 dyes. Final samples were flash frozen and stored at −80°C prior to use.

Site-directed replacement of single residues by cysteine was performed using the Stratagene (La Jolla, CA) Quikchange™ mutagenesis kit. The fidelity of all plasmids was confirmed by DNA sequencing (Agencourt Bioscience Corporation).

Creation of biotin acceptor peptide tagged PET16b

An existing BamHI restriction site was removed from the PET16b plasmid through silent modification (ACG to ACA) at position 135. The stop codon (TGA) was mutated to GGA using the Stratagene (La Jolla, CA) Quikchange™ mutagenesis kit. The biotin Acceptor Peptide (AP) sequence GLNDIFEAQKIEWHE40 and a stop codon (TGA) was then introduced using XhoI and BamHI restriction sites using primers AP-F (TCGAGGGGCTTAATGATATCTTTGAAGCTCAGAAAATTGAATGGCATGAGTGAG) and AP-R (GATCCTCACTCATGCCATTCAATTTTCTGAGCTTCAAAGATATCATTAAGCCCC).

Biotinylated protein expression

pBirAcm (AVIDITY LLC) and AP tagged PET16b were co-transformed into *E. coli* C41 (DE3). At OD_{600}=0.5, 10 mM D-biotin was added, expression was induced with 0.3mM IPTG, and cells were grown overnight at 20°C.

Scintillation Proximity-Based Binding Studies

Binding of ^{3}H-leucine (140 Ci/mmol; Moravek) to purified LeuT-variants was performed by means of the scintillation proximity assay (SPA) as described10,43 with 25 ng of purified protein per assay in buffer composed of 50 mM Tris, Mes (pH 8.0), 100 mM NaCl, 1 mM TCEP, 20% glycerol, and 1 mM DDM .

Transport and Binding in Proteoliposomes

Liposomes were prepared using *E. coli* polar lipid extract and phosphatidylcholine (Avanti) at a 3:1 (w/w) ratio as described10. Purified LeuT variants were reconstituted at a 1:150 (w/w) ratio in preformed, Triton X-100 destabilized liposomes. The accumulation of ^{3}H-Ala was measured at 23 °C in assay buffer composed of 50 mM Tris/Mes (pH 8.5), 50 mM NaCl. Binding of ^{3}H-Ala to LeuT proteoliposomes was assayed by dissipating the electrochemical NaCl gradient with 25 μg/mL gramicidin for 5 min prior to the start of the reaction. Uptake reactions were stopped by quenching the samples with ice cold assay buffer followed by rapid filtration through GF/F filters (Advantec MFS, Inc).

Steady-state fluorescence anisotropy measurements

Steady-state anisotropy measurements of Cy3-labeled LeuT (10 nM) were performed using a PTl spectrofluorometer using excitation and emission wavelengths of 532 nm and 560 nm, respectively.

Calculation of Distances from FRET Efficiencies

Distances between Cy3 and Cy5 in specific FRET states were estimated using the following equation:

$$R=R_0\sqrt[6]{\frac{1-E}{E}},$$

where R_0 is the distance at which 50% energy transfer is observed. The experimentally-determined R_0 of 58.4 Å was estimated according to the equation45:

$$R_0=0.221\sqrt[6]{\Phi_D\kappa^2\eta^{-4}J(\lambda)},$$

where refractive index of the experimental solution (η) was estimated to be 1.4 and the orientation factor, κ^2, was assumed to be 2/3 given isotropic rotation on the millisecond timescale . The spectral overlap integral $J(\lambda)=8.5\times10^{-13}$ M^{-1} cm^3 was calculated using the normalized fluorescence emission spectrum of Cy3-7C-LeuT and the absorption spectrum of Cy5-7C-LeuT collected using bulk fluorescence instrumentation (Photon Technologies). Cy3 and Cy5 extinction coefficients used in calculation46 were: $\varepsilon_{550(Cy3)}$=150,000 $M^{-1}cm^1$ and $\varepsilon_{650(Cy5)}$=250,000 $M^{-1}cm^{-1}$.

The donor quantum yield of Cy3-7C-LeuT (Φ_{Cy3}=0.23) was estimated using the comparative method47 using Rhodamine 101 in ethanol as a standard ($\Phi_{R101}\approx1.0$)48. Fluorescence emission spectra of both dyes were collected with excitation at 520 nm using constant illumination intensity and slit widths. Cy3 quantum yield was calculated as follows:

$$\Phi_{cy3}=\Phi_{Rh101}*\left(\frac{F_{cy3}}{F_{R101}}\right)*\left(\frac{A_{R101}}{A_{cy3}}\right)*\left(\frac{\eta_{cy3}}{\eta_{Rh101}}\right)^2,$$

where F_{Cy3} and F_{R101} are the integrated fluorescence emission spectra; A_{Cy3} and A_{R101} are the absorbances; and η_{Cy3}=1.4 and η_{R101}=1.36 are the refractive indexes of the solutions used for Cy3-LeuT (the buffer used for single-molecule experiments) and Rhodamine 101 (ethanol), respectively.

Single-molecule FRET experiments

Fluorescence data were acquired using a prism-based total internal reflection (TIR) microscope as previously described34. All experiments were performed in buffer containing 50 mM Tris/MES (pH 7.5), 10% glycerol, 0.02% [wt/vol] DDM, 5 mM 2-mercaptoethanol, and 200 mM salt (KCl or NaCl, as specified). An oxygen scavenging environment (1 unit/μl glucose oxidase, 8 units/μl catalase, 0.1% v/v glucose) containing 1 mM cyclooctatetraene was employed in all experiments to minimize photobleaching36.

Microfluidic imaging chambers passivated with a mixture of PEG and biotin-PEG49 were incubated with 0.8 μM streptavidin (Invitrogen), followed by 20 nM biotin-NTA (Biotium) charged with $NiCl_2$. Cy3/Cy5-labeled His_{10}-LeuT molecules (2nM) were surface immobilized to surface-bound Ni^{2+}. No significant surface immobilization, measured as described below, was observed in the absence of biotin-NTA (Supplementary Fig. 2).

Cy3 fluorophores were excited by the evanescent wave generated by total internal reflection of a single frequency light source (Ventus 532nm, Laser Quanta). Photons emitted from Cy3 and Cy5 were collected using a 1.2 NA 60X water-immersion objective (Nikon), where optical treatments were used to spatially separate Cy3 and Cy5 frequencies onto a cooled, back-thinned CCD (Cascade 128, Photometrics). Fluorescence data were acquired using MetaMorph software (Universal Imaging Corporation). Spectral bleed-through of Cy3 intensity on the acceptor channel was corrected by subtracting 7.5% of donor signal from the acceptor. FRET traces were calculated as: $FRET=I_{Cy5}/(I_{Cy3}+I_{Cy5})$, where I_{Cy3} and I_{Cy5} are the instantaneous Cy3 and Cy5 fluorescence intensities, respectively. Using established an procedure35, the ratio of donor and acceptor quantum yields and detection efficiencies (γ) was estimated to be close 1; therefore no correction was applied.

Analysis of smFRET traces

Analysis of fluorescence and FRET traces was achieved using automated analysis software (D.S. Terry, M.B. Feldman, R.B. Altman, S.C. Blanchard, manuscript in preparation), where traces were selected using algorithms implemented in MATLAB (MathWorks). Properties were calculated for each trace, and selected for further analysis if the following specific criteria were met: a single photobleaching event, at least 8:1 signal-to-background noise ratio (SNR), less than 4 donor fluorophore blinking events, a donor-to-acceptor Pearson's correlation coefficient < 0.5, and a lifetime of at least 15 frames showing FRET ≥ 0.15. Photobleaching events were detected in each trace as a significant (≥3 standard deviations of background noise) drop in the median-filtered (window size of 9 frames) total fluorescence intensity ($I_{Total}=I_{Cy3}+I_{Cy5}$) without a return to the previous average level. Events where fluorescence intensity did return were marked as blinking events. Signal-to-noise ratios are calculated as total intensity relative to the standard deviation of background noise: I_{Total}/

stdev(I_{Cy3})+stdev(I_{Cy5}). Data points corresponding to donor fluorophore dark states were excluded from calculation of the correlation coefficient.

To simplify the presentation of FRET histograms, zero-FRET states were removed following idealization of the data to a two-state model (E=0.1±0.1 and E=0.4±0.1) using segmental k-means algorithm50. Error bars in FRET histograms represent the standard deviation of 100 bootstrap samples of each set of FRET traces examined.

Kinetic parameters for biotinylated H7C-R86C-LeuT samples were estimated by manually selecting traces showing at least one transition between clearly distinct states with anti-correlated changes in donor and acceptor fluorescence intensity in each transition. The data were then idealized using a three state model (E=0±0.1, E=0.49±0.09, and E=0.75±0.07) with FRET parameters estimated by fitting smFRET histograms obtained in the absence of Na^+ to Gaussian functions. Initial rates were set to 0.05 sec^{-1}, as estimated from visual inspection of FRET traces. Average dwell times in each FRET state were estimated using a maximum likelihood algorithm51.

Molecular Dynamics

Simulations were performed on the system prepared as described10. Briefly, it consisted of over 77,000 atoms, including the explicit membrane model, solvating water molecules, and the various ions and ligands. Each of the simulations was started from the end of the previously described SMD trajectory in which the ligand in the S1 site was pulled towards the intracellular side and had reached 8–10 Å below the S1 binding site 10. The MD simulations were carried out with the NAMD program under constant temperature (310 K) and constant pressure (1 atm) (NPT) conditions. The equilibrations were long (150 ns), to achieve a suitable relaxation of the system. Two independent runs were carried out for the system, for consistency and convergence check. The results of one run are compared in Fig. 3 with those of a control run10 starting from the crystal structure (PDB:2A65, in an inward-closed state), to illustrate the level of stability and fluctuation of the system under the simulation conditions.

Supplementary Material

Refer to Web version on PubMed Central for supplementary material.

Acknowledgements

We are grateful to R. Altman for his assistance with reagents for single-molecule experiments, F. Carvalho for the preparation of membranes, J. Munro for assistance measuring anisotropy, R.Dave for preliminary photobleaching optimization studies, and M. Quick for helpful discussion and comments on the manuscript. Molecular graphic figures and movies were prepared with PyMOL (DeLano Scientific, http://www.pymol.org). Computations were performed on Ranger at the Texas Advanced Computing Center (TG-MCB090022) and the David A. Cofrin computational infrastructure of the Institute for Computational Biomedicine at Weill Cornell Medical College. This work was supported in part by National Institutes of Health Grants DA17293 and DA022413 (JAJ), DA12408 (HW), and DA023694 (LS). D.S.T. is supported by the Tri-Institutional Training Program in Computational Biology and Medicine.

References

1. Amara SG, Sonders MS. Neurotransmitter transporters as molecular targets for addictive drugs. Drug Alcohol Depend. 1998; 51(1–2):87–96. [PubMed: 9716932]
2. Rudnick, G. Mechanisms of biogenic amine neurotransmitter transporters. 2nd ed.. Totowa, New Jersey: Humana Press Inc; 2002.
3. Sonders MS, Quick M, Javitch JA. How did the neurotransmitter cross the bilayer? A closer view. Curr Opin Neurobiol. 2005; 15(3):296–304. [PubMed: 15919190]
4. Gu H, Wall SC, Rudnick G. Stable expression of biogenic amine transporters reveals differences in inhibitor sensitivity, kinetics, and ion dependence. J Biol Chem. 1994; 269(10):7124–7130. [PubMed: 8125921]
5. Torres GE, Gainetdinov RR, Caron MG. Plasma membrane monoamine transporters: structure, regulation and function. Nat Rev Neurosci. 2003; 4(1):13–25. [PubMed: 12511858]
6. Krause S, Schwarz W. Identification and selective inhibition of the channel mode of the neuronal GABA transporter 1. Mol Pharmacol. 2005; 68(6):1728–1735. [PubMed: 16150932]
7. Iversen L. Neurotransmitter transporters and their impact on the development of psychopharmacology. Br J Pharmacol. 2006; 147(Suppl 1):S82–S88. [PubMed: 16402124]
8. Beuming T, Shi L, Javitch JA, Weinstein H. A comprehensive structure-based alignment of prokaryotic and eukaryotic neurotransmitter/Na+ symporters (NSS) aids in the use of the LeuT structure to probe NSS structure and function. Mol Pharmacol. 2006; 70(5):1630–1642. [PubMed: 16880288]
9. Yamashita A, et al. Crystal structure of a bacterial homologue of Na+/Cl−-dependent neurotransmitter transporters. Nature. 2005; 437(7056):215–223. [PubMed: 16041361]
10. Shi L, et al. The mechanism of a neurotransmitter:sodium symporter--inward release of Na+ and substrate is triggered by substrate in a second binding site. Mol Cell. 2008; 30(6):667–677. [PubMed: 18570870]
11. Zhou Z, et al. LeuT-desipramine structure reveals how antidepressants block neurotransmitter reuptake. Science. 2007; 317(5843):1390–1393. [PubMed: 17690258]
12. Singh SK, Yamashita A, Gouaux E. Antidepressant binding site in a bacterial homologue of neurotransmitter transporters. Nature. 2007; 448(7156):952–956. [PubMed: 17687333]
13. Zhou Z, et al. Antidepressant specificity of serotonin transporter suggested by three LeuT-SSRI structures. Nat Struct Mol Biol. 2009; 16(6):652–657. [PubMed: 19430461]
14. Singh SK, Piscitelli CL, Yamashita A, Gouaux E. A competitive inhibitor traps LeuT in an open-to-out conformation. Science. 2008; 322(5908):1655–1661. [PubMed: 19074341]
15. Quick M, et al. Binding of an octylglucoside detergent molecule in the second substrate (S2) site of LeuT establishes an inhibitor-bound conformation. Proc Natl Acad Sci U S A. 2009; 106(14): 5563–5568. [PubMed: 19307590]
16. Blanchard SC. Single-molecule observations of ribosome function. Curr Opin Struct Biol. 2009; 19(1):103–109. [PubMed: 19223173]
17. Kinosita K Jr, Yasuda R, Noji H. F1-ATPase: a highly efficient rotary ATP machine. Essays Biochem. 2000; 35:3–18. [PubMed: 12471886]
18. Vale RD. Myosin V motor proteins: marching stepwise towards a mechanism. J Cell Biol. 2003; 163(3):445–450. [PubMed: 14610051]
19. Peterman EJ, Sosa H, Moerner WE. Single-molecule fluorescence spectroscopy and microscopy of biomolecular motors. Annu Rev Phys Chem. 2004; 55:79–96. [PubMed: 15117248]
20. Ishii Y, Nishiyama M, Yanagida T. Mechano-chemical coupling of molecular motors revealed by single molecule measurements. Curr Protein Pept Sci. 2004; 5(2):81–87. [PubMed: 15078219]
21. Zhuang X. Single-molecule RNA science. Annu Rev Biophys Biomol Struct. 2005; 34:399–414. [PubMed: 15869396]
22. Cornish PV, Ha T. A survey of single-molecule techniques in chemical biology. ACS Chem Biol. 2007; 2(1):53–61. [PubMed: 17243783]
23. Park H, Toprak E, Selvin PR. Single-molecule fluorescence to study molecular motors. Q Rev Biophys. 2007; 40(1):87–111. [PubMed: 17666122]

24. Ha T. Need for speed: mechanical regulation of a replicative helicase. Cell. 2007; 129(7):1249–1250. [PubMed: 17604712]
25. Schuler B, Eaton WA. Protein folding studied by single-molecule FRET. Curr Opin Struct Biol. 2008; 18(1):16–26. [PubMed: 18221865]
26. Herbert KM, Greenleaf WJ, Block SM. Single-molecule studies of RNA polymerase: motoring along. Annu Rev Biochem. 2008; 77:149–176. [PubMed: 18410247]
27. Wen JD, et al. Following translation by single ribosomes one codon at a time. Nature. 2008; 452(7187):598–603. [PubMed: 18327250]
28. Pyle AM. Translocation and unwinding mechanisms of RNA and DNA helicases. Annu Rev Biophys. 2008; 37:317–336. [PubMed: 18573084]
29. Noskov SY, Roux B. Control of ion selectivity in LeuT: two Na+ binding sites with two different mechanisms. J Mol Biol. 2008; 377(3):804–818. [PubMed: 18280500]
30. Celik L, Schiott B, Tajkhorshid E. Substrate binding and formation of an occluded state in the leucine transporter. Biophys J. 2008; 94(5):1600–1612. [PubMed: 18024499]
31. Jorgensen AM, Tagmose L, Bogeso KP, Peters GH. Molecular dynamics simulations of Na+/Cl(−)-dependent neurotransmitter transporters in a membrane-aqueous system. ChemMedChem. 2007; 2(6):827–840. [PubMed: 17436258]
32. Kniazeff J, et al. An intracellular interaction network regulates conformational transitions in the dopamine transporter. J Biol Chem. 2008; 283(25):17691–17701. [PubMed: 18426798]
33. Caplan DA, Subbotina JO, Noskov SY. Molecular mechanism of ion-ion and ion-substrate coupling in the Na+-dependent leucine transporter LeuT. Biophys J. 2008; 95(10):4613–4621. [PubMed: 18708457]
34. Munro JB, Altman RB, O'Connor N, Blanchard SC. Identification of two distinct hybrid state intermediates on the ribosome. Mol Cell. 2007; 25(4):505–517. [PubMed: 17317624]
35. Roy R, Hohng S, Ha T. A practical guide to single-molecule FRET. Nat Methods. 2008; 5(6):507–516. [PubMed: 18511918]
36. Dave R, Terry DS, Munro JB, Blanchard SC. Mitigating unwanted photophysical processes for improved single-molecule fluorescence imaging. Biophys J. 2009; 96(6):2371–2381. [PubMed: 19289062]
37. Bennett ER, Su H, Kanner BI. Mutation of arginine 44 of GAT-1, a (Na(+) + Cl(−))-coupled gamma-aminobutyric acid transporter from rat brain, impairs net flux but not exchange. J Biol Chem. 2000; 275(44):34106–34113. [PubMed: 10926932]
38. Shaffer PL, Goehring A, Shankaranarayanan A, Gouaux E. Structure and mechanism of a Na+-independent amino acid transporter. Science. 2009; 325(5943):1010–1014. [PubMed: 19608859]
39. Lockless SW, Ranganathan R. Evolutionarily conserved pathways of energetic connectivity in protein families. Science. 1999; 286(5438):295–299. [PubMed: 10514373]
40. Beckett D, Kovaleva E, Schatz PJ. A minimal peptide substrate in biotin holoenzyme synthetase-catalyzed biotinylation. Protein Sci. 1999; 8(4):921–929. [PubMed: 10211839]
41. Majumdar DS, et al. Single-molecule FRET reveals sugar-induced conformational dynamics in LacY. Proc Natl Acad Sci U S A. 2007; 104(31):12640–12645. [PubMed: 17502603]
42. Nie Y, Sabetfard FE, Kaback HR. The Cys154-->Gly mutation in LacY causes constitutive opening of the hydrophilic periplasmic pathway. J Mol Biol. 2008; 379(4):695–703. [PubMed: 18485365]

Methods References

43. Quick M, Javitch JA. Monitoring the function of membrane transport proteins in detergent-solubilized form. Proc Natl Acad Sci U S A. 2007; 104(9):3603–3608. [PubMed: 17360689]
44. Schaffner W, Weissmann C. A rapid, sensitive, and specific method for the determination of protein in dilute solution. Anal Biochem. 1973; 56(2):502–514. [PubMed: 4128882]
45. Lakowicz, JR. Principles of Fluorescence Spectroscopy. 3rd ed.. Baltimore, MD: Springer; 2006.
46. Mujumdar RB, et al. Cyanine dye labeling reagents: sulfoindocyanine succinimidyl esters. Bioconjug Chem. 1993; 4(2):105–111. [PubMed: 7873641]

47. Williams A, Winfield AS, Miller NJ. Relative fluorescence quantum yields using a computer-controlled luminescence spectrometer. Analyst. 1983; 108:1067–1071.

48. Karstens T, Kobs K. Rhodamine B and rhodamine 101 as reference substances for fluorescence quantum yield measurements. J. Phys. Chem. 1980; 84:1871–1872.

49. Blanchard SC, et al. tRNA dynamics on the ribosome during translation. Proc Natl Acad Sci U S A. 2004; 101(35):12893–12898. [PubMed: 15317937]

50. Qin F. Restoration of single-channel currents using the segmental k-means method based on hidden Markov modeling. Biophys J. 2004; 86(3):1488–1501. [PubMed: 14990476]

51. Qin F, Auerbach A, Sachs F. Estimating single-channel kinetic parameters from idealized patch-clamp data containing missed events. Biophys J. 1996; 70(1):264–280. [PubMed: 8770203]

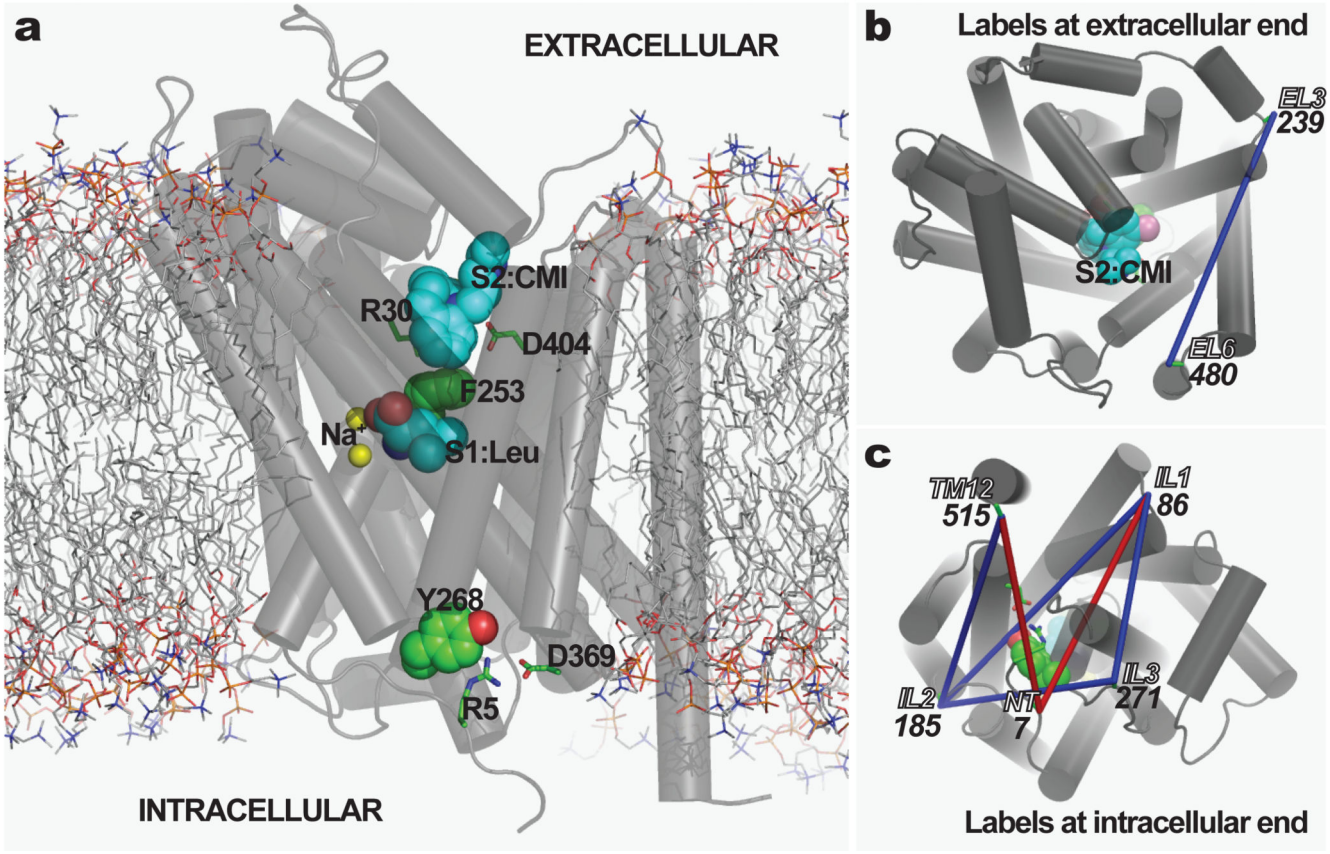

Figure 1. Structural landmarks and the disposition of the engineered Cys pairs in the crystal structure of LeuT

(**a**) Side view of the LeuT crystal structure equilibrated in a POPC lipid bilayer, showing Leu in S1, CMI in S2, sodium ions identified as yellow spheres, and the surrounding lipid molecules shown in thin stick rendering. The intracellular surface is at the bottom of the figure. Residues involved in conserved ionic:cation-π interactions in both the putative extracellular and intracellular gates are shown in volume rendering. Panels (**b**) and (**c**) indicate the Cys pairs used in this study to monitor rearrangements at the extracellular (**b**) and intracellular (**c**) ends of the transporter, under designated conditions.

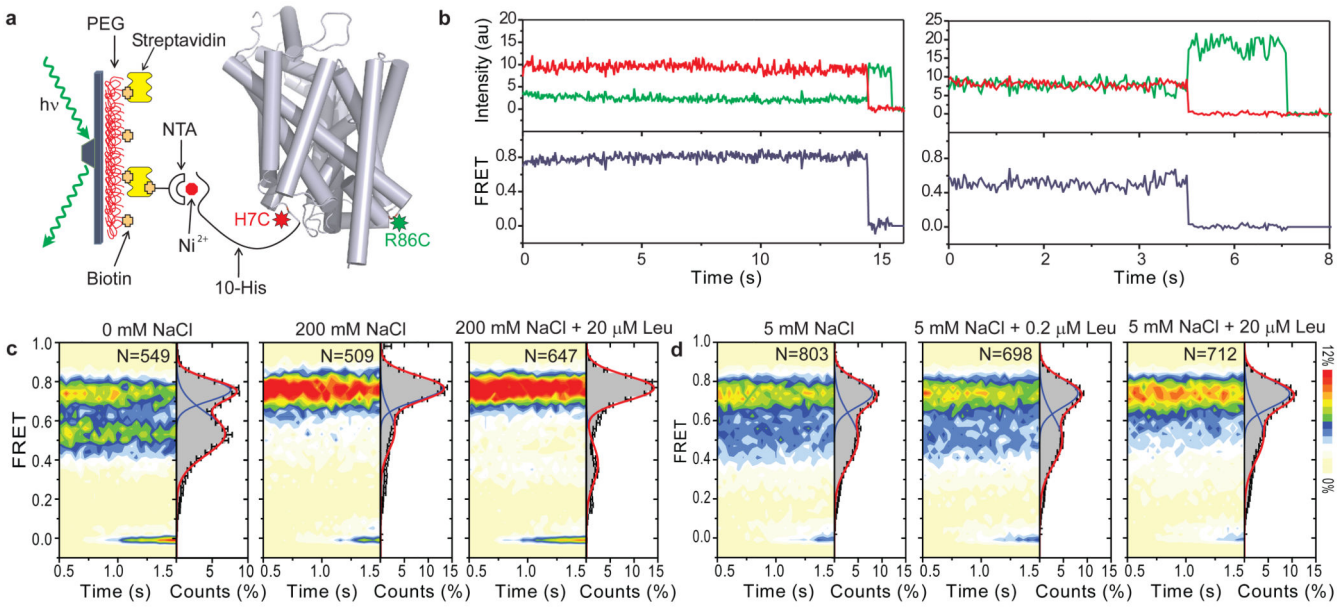

Figure 2. Single-molecule imaging of LeuT

(a) His-tagged, dye-labeled LeuT- H7C/R86C was immobilized by biotin-NTA-Ni^{2+} to the streptavidin-treated surface. **(b)** Representative fluorescence (Cy3 donor in green, Cy5 acceptor in red) and FRET (blue) time traces from experiments in 200 mM KCl. **(c)** FRET traces were summed into histograms in 200 mM KCl (left), 200 mM NaCl (center), and 200 mM NaCl with 20 μM leucine (right). Each two-dimensional histogram was summed over time (gray bars, on side), filtered to remove fluorophore dark states (see Supplementary Methods), and fit to the sum (red) of two Gaussian distributions (blue) to estimate the mean value and relative occupancies of each FRET state. **(d)** Histograms are shown for experiments performed in 5 mM NaCl with: no substrate (left), 200 nM Leu (center), and 20 μM Leu (right). Scale shown at right indicates the relative population.

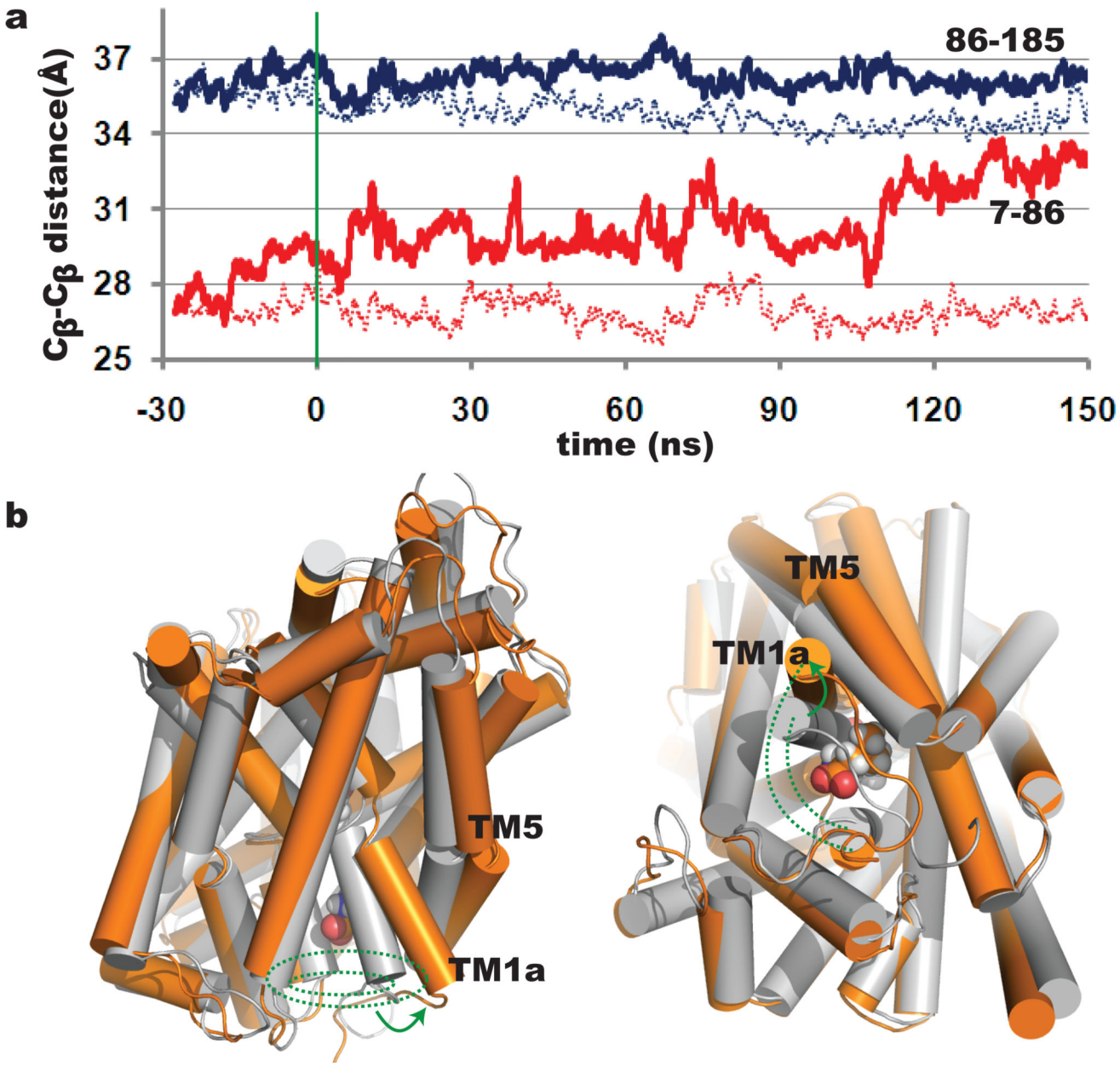

Figure 3. The structural context of the observed dynamic changes

(a) Evolution of C_β-C_β distances for specific residues observed in MD simulations in the absence (dotted lines) and presence (solid lines) of simulated transport. **(b)** Superposition of the snapshots from the MD equilibrations of the crystal structure of LeuT (gray) and the inward-open structure (orange) indicating the conformational rearrangements predicted from the MD simulations in the transport mechanism (see Supplemental Movie). In this MD frame, the descending Leu substrate is shown near the site of intracellular opening, where the proposed TM1a rearrangement is indicated by arrows. The left and right panels show views parallel to the membrane and from the intracellular side, respectively. The dotted lines comprising the intracellular ends of the same TMs that surround the exiting substrate in the

open-inward structure obtained through simulation (orange) yield larger circumference than in the crystal structure (gray).

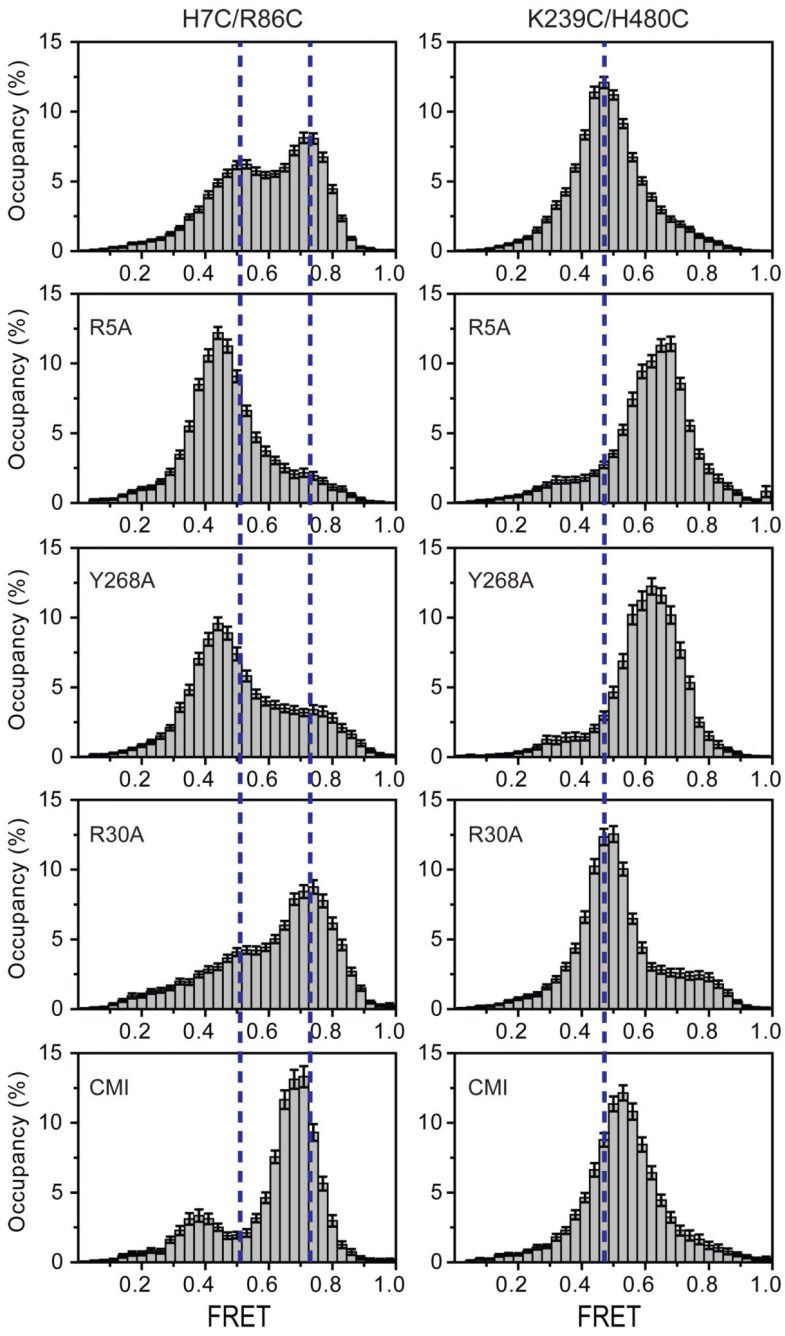

Figure 4. Effects of mutation and CMI on FRET histograms of LeuT-H7C/R86C and LeuT-239C/480C

FRET histograms from single-molecule traces obtained in the presence of 200 mM KCl for LeuT-H7C/R86C (left) and LeuT-239C/H480C (right) are shown in the context of the mutations R5A, Y268A, R30A or the presence of 0.5 mM CMI. For clarity, fluorophore dark states have been computationally removed from all histograms (Supplementary Methods).

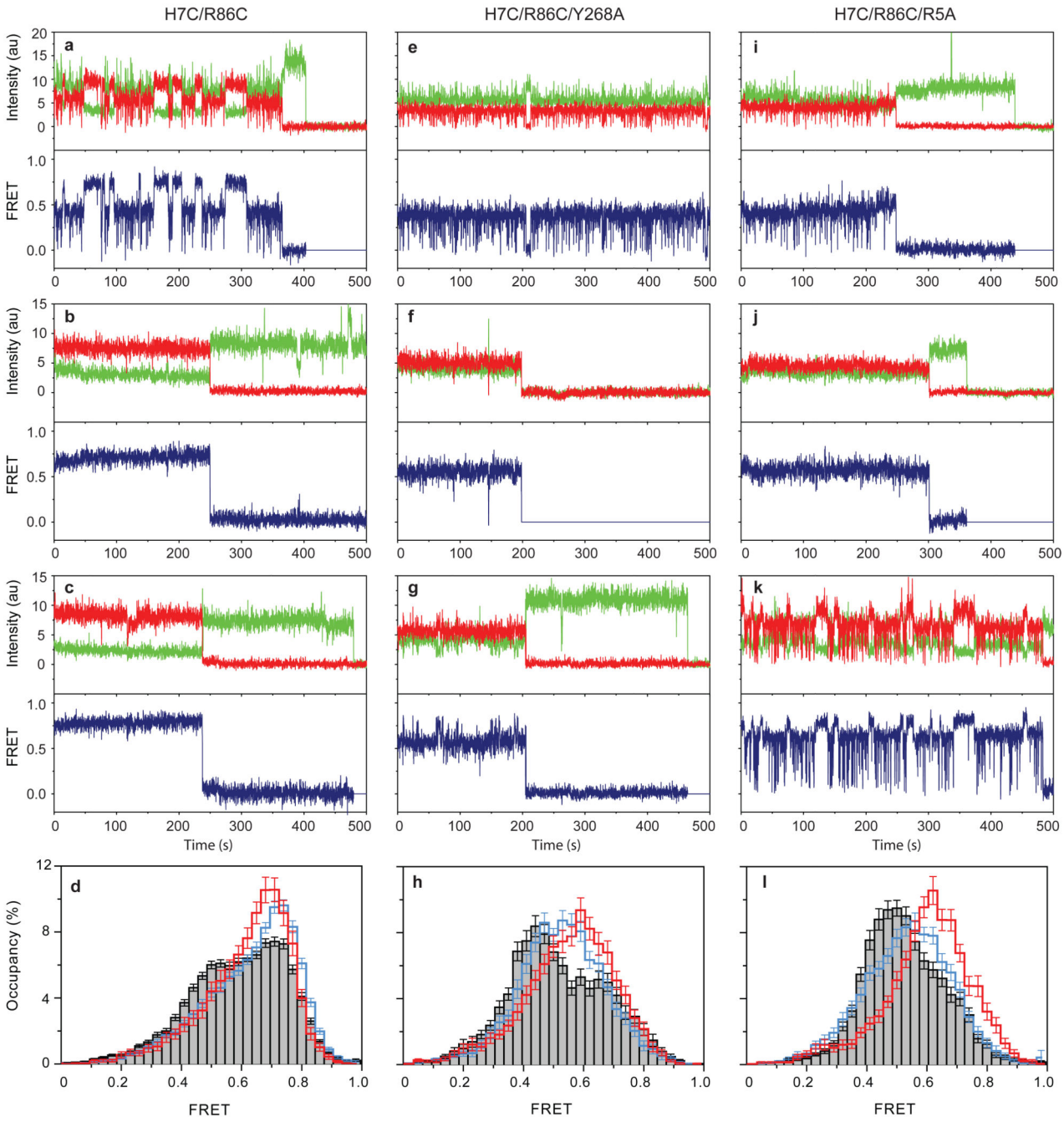

Figure 5. Long single-molecule trajectories reveal FRET transitions

Representative single-molecule traces from 160 ms images are shown for LeuT-H7C/R86C (left), LeuT-H7C/R86C/Y268A (center), and LeuT-H7C/R86C/R5A (right) in 200 mM KCl **(a, e, i)**, 200 mM NaCl **(b, f, j)** or 200 mM NaCl and 20 μM Leu **(c, g, k)**. Cy3 (donor) and cy5 (acceptor) fluorescence are shown in green and red respectively. FRET efficiency is shown in blue. One-dimensional histograms **(d, h, l)** represent the population data obtained

in the presence of 200 mM KCl (gray bars), 200 mM NaCl (blue line), or 200 mM NaCl and 20 μM Leu (red line).